

The Generation of Magnetic Fields and X-ray Observations

YUTAKA FUJITA¹ and TSUNEHIKO N. KATO²

¹ Department of Earth and Space Science, Graduate School of Science, Osaka University, Toyonaka, Osaka 560-0043, Japan

² National Astronomical Observatory, Osawa 2-21-1, Mitaka, Tokyo 181-8588, Japan

Received; accepted; published online

Abstract. We show that strong magnetic fields can be generated at shock waves associated with formation of galaxies or clusters of galaxies by the Weibel instability, an instability in collisionless plasmas. The estimated strength of the magnetic field generated through this mechanism is close to the order of values observed in galaxies or clusters of galaxies at present, which indicates that strong amplification of magnetic fields after formation of galaxies or clusters of galaxies is not required. This mechanism could have worked even at a redshift of ~ 10 , and therefore the generated magnetic fields may have affected the formation of stars at the early universe. This model will be confirmed by future observations of nearby clusters of galaxies. In this context, we also present the Japanese X-ray missions.

Key words: instabilities — magnetic fields — galaxies: general — galaxies: clusters: general

©0000 WILEY-VCH Verlag GmbH & Co. KGaA, Weinheim

1. Introduction

The question of the origin of galactic magnetic fields is one of the most challenging problems in modern astrophysics. It is generally assumed that magnetic fields in spiral galaxies are amplified and maintained by a dynamo through rotation of the galaxies (Widrow 2002). The dynamo requires seed fields to be amplified. However, observations of microgauss fields in galaxies at moderate redshifts strongly constrain the lower boundary of the seed fields (Athreya et al. 1998). Moreover, magnetic fields are also observed in elliptical galaxies and galaxy clusters where rotation, and thus dynamo mechanism cannot play a central role (Clarke, Kronberg & Böhringer 2001; Widrow 2002; Vallée 2004).

On the other hand, the Weibel instability can provide another mechanism to generate strong magnetic fields (Weibel 1959; Fried 1959). This instability is driven in a collisionless plasma, or a tenuous ionized gas, by the anisotropy of the particle velocity distribution function (PDF) of the plasma. When the PDF is anisotropic, currents and then magnetic fields are generated in the plasma so that the plasma particles are deflected and the PDF becomes isotropic (Medvedev & Loeb 1999). Through the instability, the free energy attributed to the PDF anisotropy is transferred to magnetic field energy. This instability does not need seed magnetic fields. It can be saturated only by nonlinear effects, and thus the

magnetic fields can be amplified to very high values. This instability has been observed directly in recent laser experiments (Wei et al. 2002). In astrophysical plasmas, the instability is expected to develop at shocks or at steep temperature gradients, where the PDF is anisotropic. Examples of the sites are pulsar winds, shocks produced by gamma-ray bursts, jets from active galactic nuclei (AGNs), cosmological shocks, and cold fronts (contact discontinuities between cold and hot gas) in clusters of galaxies (Medvedev & Loeb 1999; Kazimura et al. 1998; Nishikawa et al. 2003; Schlickeiser & Shukla 2003; Okabe & Hattori 2003). Although the instability was found in 1959, its nonlinear nature had prevented us from understanding its long-term evolution. Recently, however, as computer power increases, detailed particle simulations of plasmas have been initiated and they have revealed the evolution of magnetic fields even after saturation of the instability (Silva et al. 2003; Medvedev et al. 2005). Based on these results, we consider the generation of magnetic fields at galaxy and cluster-scale shocks through the Weibel instability at the formation of galaxies (both ellipticals and spirals) and clusters. We use the cosmological parameters of $\Omega_0 = 0.3$, $\lambda = 0.7$, the Hubble constant of $H_0 = 70 \text{ km s}^{-1} \text{ Mpc}^{-1}$, and $\sigma_8 = 0.9$.

2. Models

2.1. Generation of magnetic fields

The evolution of the Weibel instability can be understood as evolution of current filaments generated in a plasma (Medvedev et al. 2005; Kato 2005). The growth of the instability ceases once the magnitude of current in each filament reaches the Alfvén current (Kato 2005); physically this condition is consistent with the condition by Medvedev & Loeb (1999) that the particle's gyroradii in the excited magnetic fields are comparable to the characteristic wavelength of the magnetic field. In proton-electron plasmas, heavier protons mainly determine the final magnetic field strength (Frederiksen et al. 2004). Thus, we consider the generation of magnetic fields by protons. At a shock front, an anisotropy is produced in the PDF of protons owing to the difference between the shock speed u and the thermal velocity of protons v_{th} . When the shock Mach number ($\mathcal{M} = u/v_{\text{th}}$) is larger than ~ 2 , which is the case in the galactic shocks we consider later, the anisotropy becomes large enough to adopt the 'particle-limit' solution discussed by Kato (2005). In this case, the saturated magnetic field is determined only by the shock velocity and the proton number density n_p as

$$B_{\text{sat}} \approx \chi_P u \sqrt{2\pi n_p m_p}, \quad (1)$$

where m_p is the proton mass, and χ_P is the isotropization factor at the saturation, which is typically 0.5 (Kato 2005). The saturated magnetic energy density reaches a sub-equipartition level with the particle kinetic energy, which is consistent with previous simulation results under large anisotropic conditions (Yang, Arons & Langdon 1994; Califano et al. 1998)

After saturation, the magnetic field strength decreases as the current filaments merge. Recent particle simulations have shown that the final magnetic field strength is given by $B_f = \eta_{\text{mer}}^{1/2} B_{\text{sat}}$, where $\eta_{\text{mer}} \sim 0.01$ (Silva et al. 2003; Medvedev et al. 2005), thus we use this value. Long-term evolution (say Gyr) of the generated magnetic fields is still an open question. However, Medvedev et al. (2005) indicated that the fields do not decay rapidly after the saturation, because the spatial scale of the fields increases rapidly and dissipative processes such as Ohmic heating or ion-neutral collisions, if any, are suppressed. The very long-term evolution of the magnetic fields, for which the results of Medvedev et al. (2005) and Silva et al. (2003) cannot be directly applied, is discussed in Fujita and Kato (2005).

2.2. Shock formation

According to the standard hierarchical clustering scenario of the universe, an initial density fluctuation of dark matter in the universe gravitationally grows and collapses; its evolution can be approximated by that of a spherical uniform overdense region (Gunn & Gott 1972; Peebles 1980). The collapsed objects are called 'dark halos' and the gas in these objects later forms galaxies or clusters of galaxies. At the collapse, the gas is heated by the 'virial shocks' to the virial temperature of the dark halo, $T_{\text{vir}} = GM/(2r_{\text{vir}})$, where G is the gravitational constant, and M and r_{vir} are the mass and

the virial radius of the dark halo, respectively. The relation between the virial radius and the virial mass of an object is given by

$$r_{\text{vir}} = \left[\frac{3M}{4\pi\Delta_c(z)\rho_{\text{crit}}(z)} \right]^{1/3}, \quad (2)$$

where $\rho_{\text{crit}}(z)$ is the critical density of the universe and $\Delta_c(z)$ is the ratio of the average density of the object to the critical density at redshift z . In the Λ CDM cosmology, the critical density depends on redshift because the Hubble constant depends on that, and it is given by

$$\rho_{\text{crit}}(z) = \frac{\rho_{\text{crit},0}\Omega_0(1+z)^3}{\Omega(z)}, \quad (3)$$

where $\rho_{\text{crit},0}$ is the critical density at $z = 0$, and $\Omega(z)$ is the cosmological density parameter given by

$$\Omega(z) = \frac{\Omega_0(1+z)^3}{\Omega_0(1+z)^3 + \lambda} \quad (4)$$

for the flat universe with non-zero cosmological constant. The ratio $\Delta_c(z)$ is given by

$$\Delta_c(z) = 18\pi^2 + 82x - 39x^2, \quad (5)$$

for the flat universe (Bryan & Norman 1998), where the parameter x is given by $x = \Omega(z) - 1$. The virial shocks form at $r \approx r_{\text{vir}}$ and the velocity is $v_{\text{vir}} \approx \sqrt{GM/r_{\text{vir}}}$.

In addition, recent cosmological numerical simulations have shown that 'large-scale structure (LSS) shocks' form even before the gravitational collapse (Miniati et al. 2000; Ryu et al. 2003; Furlanetto & Loeb 2004); they form at the turnaround radius ($r_{\text{ta}} \sim 2r_{\text{vir}}$), the point at which the density fluctuation breaks off from the cosmological expansion. Thus, the gas that is going to form a galaxy or a cluster undergoes two types of shocks; first, the gas passes the outer LSS shock, and then, the inner virial shock. The typical velocity of the LSS shocks is $v_s \approx H(z)R_p$ (Furlanetto & Loeb 2004), where $H(z)$ is the Hubble constant at redshift z , and R_p is the physical radius that the region would have had if it had expanded uniformly with the cosmological expansion. The temperature of the postshock gas is $T_s \approx 3/16(\mu m_p/k_B)v_s^2$, where μm_p is the mean particle mass, and k_B is the Boltzmann constant. Note that we do not consider mergers of objects that have already collapsed as the sites of magnetic field generation. During the merger, collapsed objects just bring their magnetic fields to the newly born merged object.

Since the Weibel instability develops in ionized gas (plasma), we need to consider the ionization history of the universe. After the entire universe is ionized by stars and/or AGNs ($z \lesssim 8$), magnetic fields are first generated at the LSS shocks. In this case, we do not consider the subsequent generation of magnetic fields at the inner virial shocks, because the strength is at most comparable to that of the magnetic fields generated at the LSS shocks. On the other hand, when the universe is not ionized ($z \gtrsim 8$), the Weibel instability cannot develop at the outer LSS shocks. However, if the LSS shocks heat the gas (mostly hydrogen) to $T_s > 10^4$ K and ionize it, the instability can develop at the inner virial shocks.

For this case, the gas ionized at the LSS shock may recombine before it reaches the virial shock. The recombination time-scale is given by

$$\tau_{\text{rec}} = \frac{1}{\alpha n_e} \approx 1.22 \times 10^5 \text{ yr} \frac{1}{y} \left(\frac{T}{10^4 \text{ K}} \right)^{0.7} \left(\frac{n_H}{\text{cm}^{-3}} \right)^{-1}, \quad (6)$$

where α is the recombination coefficient, n_e is the electron density, T is the gas temperature, y is the ionization fraction, and n_H is the hydrogen density (Shapiro & Kang 1987). If we assume that $\tau_{\text{rec}} = \tau_{\text{dyn}}$, where $\tau_{\text{dyn}} \approx (1/2)r_{\text{ta}}/u$ is the time-scale that the gas moves from the LSS shock to the virial shock, the ionization rate when the gas reaches the virial shock is

$$y \approx \left(\frac{\tau_{\text{dyn}}}{1.22 \times 10^5 \text{ yr}} \right)^{-1} \left(\frac{T}{10^4 \text{ K}} \right)^{0.7} \left(\frac{n_H}{\text{cm}^{-3}} \right)^{-1} \quad (7)$$

for $y < 1$. We found that $y < 1$ for $z \gtrsim 9$, and the minimum value when the generation of magnetic fields is effective ($z \lesssim 12$, see §3) is $y \sim 0.3$. When $y < 1$, we simply replace n_p in equation (1) with yn_H . For temperature, we assumed $T = T_s$ in equation (7). Since the magnetic fields do not much depend on the temperature ($B_{\text{sat}} \propto y^{0.5} \propto T^{0.35}$), they do not much change even when radiative cooling reduces the temperature; at least B_{sat} does not change by many orders of magnitude. Since the ionization rate is fairly large, the ambipolar diffusion of magnetic fields can be ignored (e.g. eq. 13–57 in Spitzer 1978). It was shown that the ionization rate just behind a shock is $y \sim 0.1$, if the shock velocity is relatively small 40 km s^{-1} (Shapiro & Kang 1987; Susa et al. 1998). If the shock velocity is larger, $y \sim 1$. In our calculations, the velocity of the LSS shocks is $u \gtrsim 40 \text{ km s}^{-1}$, when the generation of magnetic fields is effective. Thus, y just behind the shocks is at least comparable to that obtained through the condition of $\tau_{\text{rec}} \sim \tau_{\text{dyn}}$, and the incomplete ionization does not much affect the results shown in the next section.

3. Results and discussion

Fig.1 shows the typical mass of objects, M , as a function of redshift z ; the labels 1σ , 2σ , and 3σ indicate the amplitudes of initial density fluctuations in the universe from which the objects form, on the assumption of the CDM fluctuations spectrum (Barkana & Loeb 2001). Fig.2 shows the downstream temperature at the virial shock (T_{vir}) and that at the LSS shock (T_s) for the objects; T_{vir} is always larger than T_s . The ratio T_{vir}/T_s indicates that $\mathcal{M} \gtrsim 4$ for the virial shock. For the LSS shock, $\mathcal{M} \gg 1$, because the gas outside the shock is cold. Thus, equation (1) can be applied to both shocks. In Fig.3, we present the strength of magnetic fields (B_c) at a scale of r_{vir} for the collapsed objects. We assume that the entire universe is reionized at $z = 8$. Thus, for $z > 8$, magnetic fields are generated only at the virial shocks if $T_s > 10^4 \text{ K}$. We assume that $B_c = B_f$ and plot the lines only when $T_s > 10^4 \text{ K}$. The recombination is effective at $z > 12$ for the 3σ model and at $z > 8$ for the 2σ model. On the other hand, for $z < 8$, the magnetic fields are generated at the LSS shocks. We consider the compression of the fields

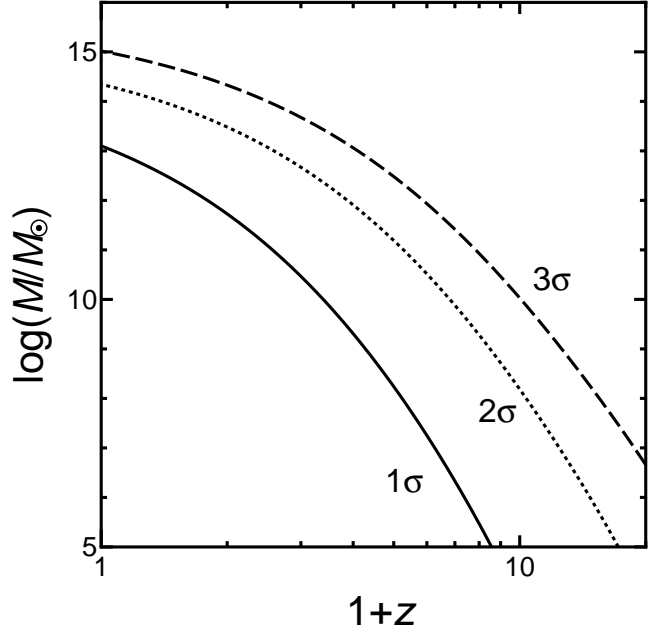


Fig. 1. Typical masses of objects forming at redshift z . The labels, 1σ , 2σ , and 3σ (solid, dotted, and dashed lines, respectively) indicate the amplitudes of initial density fluctuations from which the objects formed; $\sim 1\text{--}3\sigma$ is the typical value (Barkana & Loeb 2001). Objects with masses of $M \lesssim 10^{12} M_\odot$ and $M \gtrsim 10^{13} M_\odot$ correspond to galaxies (ellipticals and spirals) and clusters of galaxies, respectively.

while the size of the gas sphere decreases from $r = r_{\text{ta}}$ to $r = r_{\text{vir}}$, and thus we assume that $B_c = 8^{2/3} B_f$. Moreover, we plot the lines only for $T_{\text{vir}} > 2 \times 10^5 \text{ K}$, because below this temperature, gas infall is suppressed by photoionization heating (Efstathiou 1992; Furlanetto & Loeb 2004).

In Fig.3, the strength of magnetic fields reaches $\sim 10^{-8}\text{--}10^{-7} \text{ G}$, which is very close to the values observed in nearby galaxies and clusters of galaxies ($\sim 10^{-6} \text{ G}$; Clarke et al. 2001; Widrow 2002; Vallée 2004). This indicates that strong amplification of magnetic fields, such as dynamo amplification, is not required after formation of the galaxies and clusters. The absence of a strong amplification is consistent with the observations of galactic magnetic fields at $z \gtrsim 2$ (Athreya et al. 1998). Future observations of higher-redshift galaxies would discriminate between our model and strong dynamo amplification models; the latter predict much weaker magnetic fields at higher redshifts. Moreover, since the predicted galactic magnetic fields are comparable to those at present, they might have affected the formation of stars in protogalaxies. Fig.3 also shows that our model naturally explains the observational fact that the magnetic field strengths of galaxies and galaxy clusters fall in a small range (a factor of 10). Since our model predicts that magnetic fields are generated around objects, magnetic fields in intergalactic space are not required as the seed or origin of galactic magnetic fields.

Although it would be difficult to directly observe the generation of magnetic fields through the Weibel instability for distant high-redshift galaxies, it would be easier for nearby clusters of galaxies. Since clusters are now in the forma-

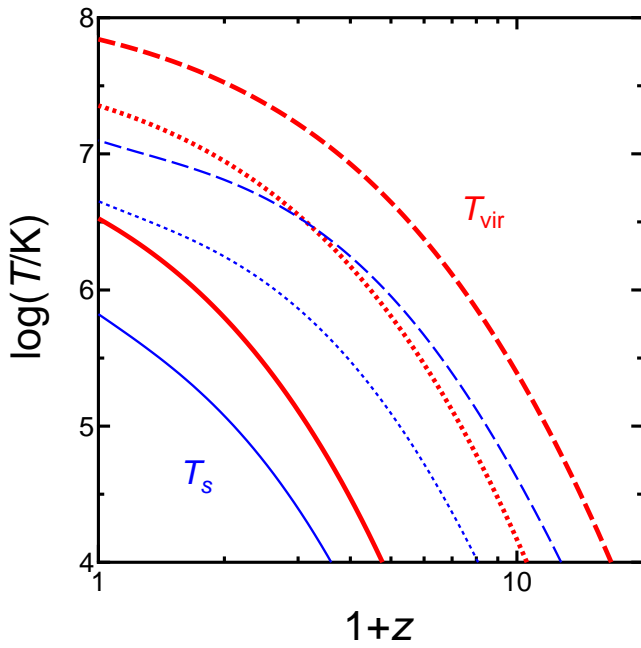


Fig. 2. Temperatures behind the virial shocks (T_{vir} ; thick lines) and those behind the LSS shocks (T_s ; thin lines) for objects forming at redshift z (Fujita & Kato 2005). Solid, dotted, and dashed lines correspond to 1σ , 2σ , and 3σ fluctuations, respectively (see Fig.1)

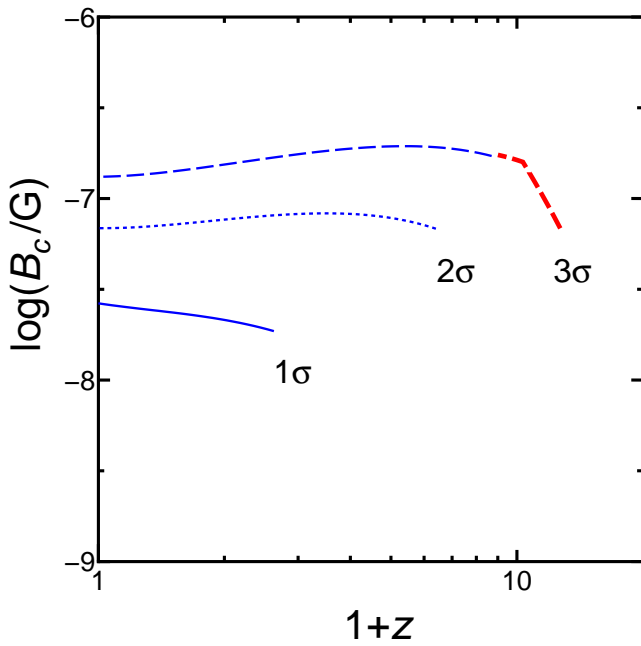


Fig. 3. Typical magnetic field strengths of objects forming at redshift z (Fujita & Kato 2005). Solid, dotted, and dashed lines correspond to 1σ , 2σ , and 3σ fluctuations, respectively (see Fig.1).

tion process, LSS shocks should be developing outside of the virial radii of the clusters (Miniati et al. 2000; Ryu et al. 2003). Since particles are often accelerated at shocks, the synchrotron emission from the accelerated particles could be observed with radio telescopes with high sensitivity at low frequencies (Keshet, Waxman & Loeb 2004). The total non-thermal luminosity due to synchrotron luminosity plus inverse Compton scattering with cosmic microwave background (CMB) photons is estimated as

$$L_{\text{nt}} \approx \frac{\epsilon}{r_{\text{ta}}/u} \frac{fM}{m_p} \frac{1}{2} u^2, \quad (8)$$

where ϵ is the acceleration efficiency and f is the gas fraction of a cluster. If we assume $\epsilon = 0.03$ and $f = 0.15$, the maximum value of L_{nt} is $\sim 10^{43}$ erg s $^{-1}$. Since the energy density of magnetic fields (u_B) is smaller than that of the CMB (u_{CMB}), most of the non-thermal luminosity (L_{nt}) is attributed to the inverse Compton scattering such as $u_{\text{CMB}} L_{\text{nt}} / (u_B + u_{\text{CMB}})$, which may have been detected in the hard X-ray band ($\gtrsim 20$ keV; Fusco-Femiano et al. 2004). Thus, the synchrotron radio luminosity is $u_B L_{\text{nt}} / (u_B + u_{\text{CMB}}) \lesssim 10^{41}$ erg s $^{-1}$. Some of the diffuse radio sources observed in the peripheral cluster regions ('radio relics') may be this emission (Govoni & Feretti 2004). Since the Weibel instability generates magnetic fields on the plane of the shock front, the synchrotron emission should be polarized perpendicular to the shock front (Medvedev & Loeb 1999), which is actually observed for some radio relics (Govoni & Feretti 2004). The synchrotron emission will tell us the positions of the LSS shocks, if they exist. If magnetic fields are generated there, they should be observed only downstream of the shock. This may be confirmed through Faraday rotation measurements of radio sources behind the cluster for both sides of the shock, if the coherent length of the fields sufficiently increases.

4. Japanese X-ray missions

4.1. Suzaku (Astro-E2)

Suzaku is the recovery mission for *ASTRO-E*, which did not achieve orbit during the launch in 2000. *Suzaku* was launched in July 10, 2005. *Suzaku* has three detectors (*XRS*, *XIS*, and *HXD*). *XRS* has a superb energy resolution ($\lesssim 6.5$ eV ~ 100 km s $^{-1}$). We expected that it could detect gas motion in clusters, for example. *XRS* uses liquid helium to cool the detector. Unfortunately, the helium evaporated before the first light (Aug.8) and *XRS* was lost. The cause of the trouble is now under investigation. The observation schedule will be changed and optimized to the remaining two detectors (*XIS* and *HXD*). *XIS* has imaging capability and its energy range is 0.2–12 keV. *HXD* is a hard X-ray detector and its energy range is 10–600 keV. *XIS* and *HXD* are working well. Their sensitivities are shown in Figure 4. It is to be noted that the background levels of these detectors are lower than those of *Chandra* and *XMM-Newton*. *XIS* and *HXD* will give us various information in the field of high energy astrophysics (e.g.

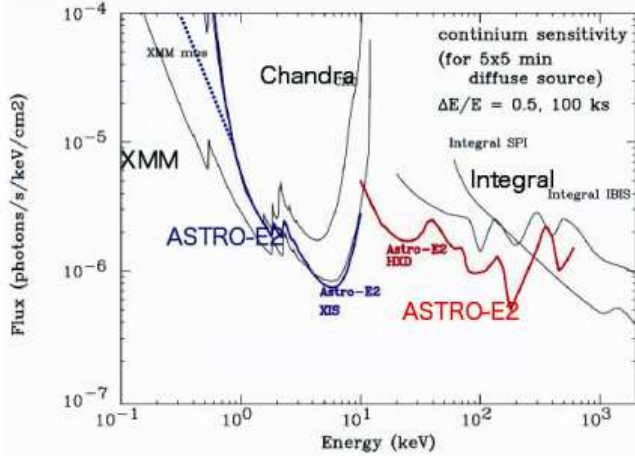


Fig. 4. The sensitivities of *Suzaku* (*Astro-E2*) and other satellites.

hard X-ray from black holes and clusters of galaxies). Readers can get the information on *Suzaku* at several web sites.¹

4.2. NeXT

NeXT (*New X-ray Telescope*) is the major Japanese X-ray mission after *Suzaku*.² If the plan is approved, *NeXT* will be launched in 2011, before the launch of *Constellation-X* and *XEUS*. *NeXT* will have imaging capability in the hard X-ray band. For example, we will easily get the images of radio relics in clusters of galaxies by observing their inverse Compton emission (Figure 5). The sensitivity will be much higher than those of previous satellites (Figure 6). *NeXT* will also have an ultra-high resolution soft X-ray spectrometer, which will be another challenge of *Suzaku XRS*. Moreover, *NeXT* will have a soft gamma-ray detector. Thus, it will enable us to observe objects in a very wide energy band.

Acknowledgements. We thank K. Omukai, N. Okabe, T. Kudoh, K. Asano, S. Inoue, K. Nakazawa, and H. Matsumoto for discussions. Y. F. is supported in part by a Grant-in-Aid from the Ministry of Education, Culture, Sports, Science, and Technology of Japan (14740175).

References

Athreya, R. M., Kapahi, V. K., McCarthy, P. J., van Breugel, W.: 1998, *A&A* 329, 809

Barkana, R., Loeb A.: 2001, *PhR* 349, 125

Bryan, G. L., Norman, M. L.: 1998, *ApJ* 495, 80

Califano, F., Pegoraro, F., Bulanov, S. V., Mangeney, A.: 1998, *PhRvE* 57, 7048

Clarke, T. E., Kronberg, P. P., Böhringer, H.: 2001, *ApJ* 547, L111

Efstathiou, G.: 1992, *MNRAS* 256, 43P

Frederiksen, J. T., Hededaal, C. B., Haugbølle, T., Nordlund, Å.: 2004, *ApJ* 608, L13

Fried, B. D.: 1959, *PhFl* 2, 83

Fujita, Y., Kato, T. N.: 2005 *MNRAS* 364, 247

Furlanetto, S. R., Loeb, A.: 2004, *ApJ* 611, 642

Fusco-Femiano, R., Orlandini, M., Brunetti, G., Feretti, L., Giovannini, G., Grandi, P., Setti, G.: 2004, *ApJ* 602, L73

Gunn, J. E., Gott, J. R. I.: 1972, *ApJ* 176, 1

Govoni, F., & Feretti, L.: 2004, *Int. J. Mod. Phys. D* 13 1549

Kato, T. N.: 2005, *PhPl* 12, 080705

Kazimura, Y., Sakai, J. I., Neubert, T., Bulanov, S. V.: 1998, *ApJ* 498, L183

Keshet, U., Waxman, E., & Loeb, A.: 2004, *ApJ* 617, 281

Medvedev, M. V., Fiore, M., Fonseca, R. A., Silva, L. O., Mori, W. B.: 2005, *ApJ* 618, L75

Medvedev, M. V., Loeb, A.: 1999, *ApJ* 526, 697

Miniati, F., Ryu, D., Kang, H., Jones, T. W., Cen, R., Ostriker, J. P.: 2000, *ApJ* 542, 608

Nishikawa, K.-I., Hardee, P., Richardson, G., Preece, R., Sol, H., Fishman, G. J.: 2003, *ApJ* 595, 555

Okabe, N., Hattori, M.: 2003, *ApJ* 599, 964

Peebles, P. J. E. 1980, *Large-Scale Structure of the Universe* (Princeton Univ. Press; Princeton)

Ryu, D., Kang, H., Hallman, E., Jones, T. W.: 2003, *ApJ* 593, 599

Schlickeiser, R., Shukla, P. K.: 2003, *ApJ* 599, L57

¹ <http://www.isas.jaxa.jp/e/enterp/missions/astro-e2/>

² <http://heasarc.gsfc.nasa.gov/docs/astroe/astroe2.html>

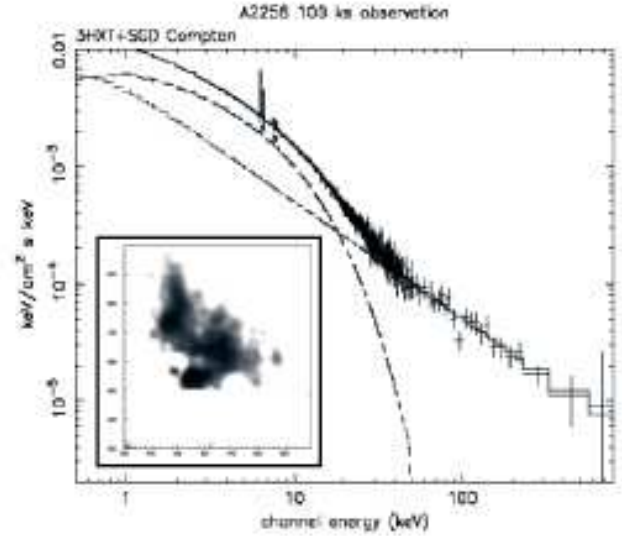


Fig. 5. A simulated hard X-ray image and the spectrum of the radio relic in Abell 2256 observed by *NeXT*.

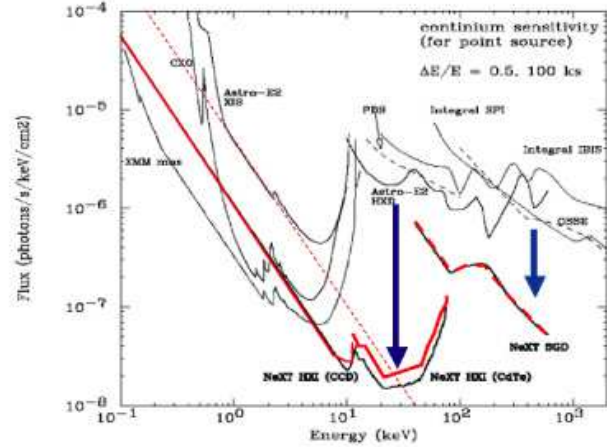


Fig. 6. The aimed sensitivity of *NeXT* and the sensitivities of other satellites.

Shapiro, P. R., Kang, H.: 1987, *ApJ* 318, 32

Silva, L. O., Fonseca, R. A., Tonge, J. W., Dawson, J. M., Mori, W. B., Medvedev, M. V.: 2003, *ApJ* 596, L121

Spitzer, L. 1978, *Physical Processes in the Interstellar Medium* (New York: Wiley)

Susa, H., Uehara, H., Nishi, R., Yamada, M. 1998, *PThPh* 100, 63

Vallée, J. P.: 2004, *NewAR* 48, 763

Wei, M. S., et al.: 2002, Central Laser Facility (UK) Annual Report (<http://www.clf.rl.ac.uk/Reports/2001-2002/pdf/10.pdf>)

Weibel, E. S.: 1959, *PhRvL* 2, 83

Widrow, L. M.: 2002, *RvMP* 74, 775

Yang, T.-Y. B., Arons, J., Langdon, A. B.: 1994, *PhPl* 1, 3059